Toward Scalable, Automated Tower-Top Phased Array Calibration

Tim Cooper, Justine McCormack, Ronan Farrell and Gerard Baldwin
Centre for Telecommunications Value-Chain Research (CTVR)
Institute of Microelectronics and Wireless Systems
National University of Ireland, Maynooth
Co. Kildare, Ireland
Email: tcooper@eeng.nuim.ie

***Abstract*— The tower-top deployment of base station electronics could prove of utility in future cellular communication applications. We present a scalable, non-radiative, automated calibration scheme for such a system, which employs an array of independently phased transceivers. By coupling an interlinear row of reference transceivers to the array, feedpoint calibration of the array is possible. The theoretical justification for the scheme is presented together with assessment of the accuracy of calibration possible using commercial off the shelf components.**

I. Introduction

The principle motivation behind relocation of the base station electronics to the tower top are the versatility, performance and space saving benefits such a system would yield. The use of a tower-top base station may also reduce capital costs because the need for both feeder cables and large resonant cavity duplexer filters is obviated. There are, however, many significant engineering challenges to the implementation of such a scheme. One of the most significant is obtaining the same RF output power as that of a conventional, tower-bottom, system. We conject that the RF system specifications will be easier to meet in the distributed tower-top system of figure 1, wherein, the RF transceiver electronics are distributed amongst the individual array elements. Appropriate summation and weighting is performed within a tower-top controller unit. The remaining demodulation functions are then performed by a tower-bottom baseband radio.

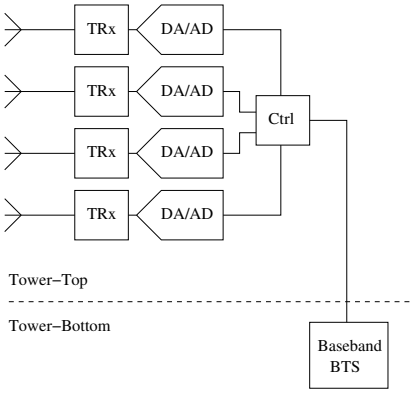

Fig. 1. A single sector of the tower-top system sees the transceiver electronics distributed between each element (here four are shown) within the array.

This distribution between array elements will allow the transition to lower cost ceramic duplexers [1] because, given an element gain of 5 dBi, a directional 30 element array would require feed-point power of 3.2 W to meet the current GSM specification. It is anticipated that this will also assist meeting the stringent reliability requirements and heat dissipation performance needed of a tower-top radio. Whether such a transceiver can be implemented, and produced affordably, remains the subject of continued interest.

The aforementioned benefits are offset by several disadvantages. The two most pertinent are reliability and accurate phasing of the array, also known as 'the calibration problem'. It is the latter of these two problems which this paper addresses in the context of a tower-top cellular system. Aspects of this calibration scheme are protected by patent pending (S2006/0482).

II. Array Calibration

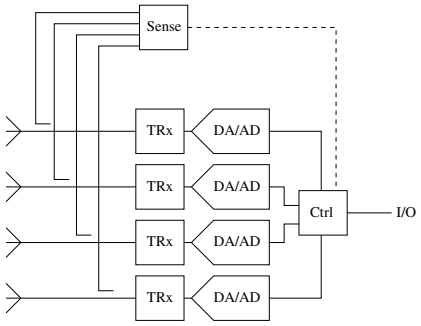

Fig. 2. Conventional array calibration wherein a coupled feedback path allows measurement of the transmitted signal and injection of calibration signals.

Where calibration is non-radiative, i.e. does not employ remote or local signals radiated in free space as the main calibration medium then array calibration, typically, is based on a closed feedback loop between a single sensing device and the outputs of the array, as shown in figure 2. It is well known that calibration relative to a single reference element, by means of weighting the input to the array, can yield accurate amplitude and phasing at the antenna feedpoint. This is usually

conditional upon the paths between the antenna feed point and reference element being equal and that the transceiver local oscillators are frequency coherent. Potential difficulties with this type of calibration scheme are that, in scaling it to arrays of significant dimensions, such as those which could be required to make a tower-top cellular transceiver, can give rise to complex calibration coupler arrangements which must be carefully designed to avoid unwanted coupling and electrical path length imbalance.

III. Interlinear Reference Calibration

To accommodate larger numbers of array elements, each with a separate transceiver, the calibration scheme shown in figure 3 is proposed. Here each group of four transceivers is coupled to a central sensing device capable of generating or receiving calibration signals for both transmit or receive band calibration. This coupling is achieved here by a hypothetical six port directional coupler structure. The output of the sensing electronics is therefore terminated in a matched impedance Z.

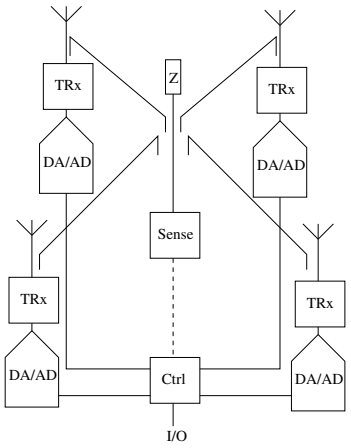

Fig. 3. Calibration relative to a single central sensing element equidistant from the neighboring radiative transceivers. Calibration is applied through the conventional feedback mechanisms.

For the purpose of this paper we will describe only transmit calibration although, by reciprocity, receive calibration is also possible. For transmitter calibration, the role of the central sensing element is to perform feed-point measurements of the transmitter phase and amplitude via the coupler structure. Thus allowing direct comparison of the feedpoint signals of each of the array's transmitters. To effect calibration, one of the radiative transmitter elements is selected to calibrate the rest of the array relative to, say, the bottom left. Our reference sensor then records the phase and amplitude of the coupled signal from that transmitter. Each of the other three elements then have their output sampled in turn, by the same reference sensor. It is then a simple matter to apply a corrective digital baseband weighting to each of the three transmitter inputs, such that their outputs - as measured by our reference, are all equal to that of the bottom left hand element. Thus enabling accurate phasing of the array.

By repeating this tessellating coupler structure (see figure 4 a) the calibration scheme may, in principal, be scaled to arrays of any proportions - each group of four transceivers being calibrated relative to a central 'reference' element (which contains the control and sensing functionality of previous figures). This process is repeated across the whole array with each transceiver being calibrated relative to a previously calibrated array element until the whole array is accurately phased.

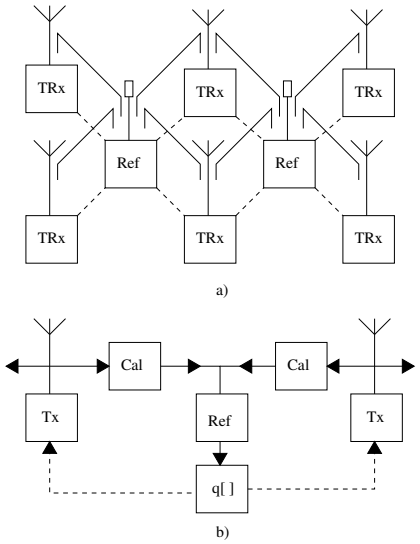

Fig. 4. a) Arrangement of coupler and sensing elements to calibrate a rectilinear array. b) Block schematic representation of the linear array calibration simulation.

A system level schematic representation of the calibration process, simplified to a linear array, is shown in figure 4 b). Here a uniform linear array is calibrated by a row of reference elements (Ref) placed between the adjacent radiative transmitters (Tx) which form the array. The transmitted signal from the first transceiver is coupled via the calibration coupler network (Cal) to a reference element[1]. This measurement is subsequently compared with measurements from neighboring elements and the transmitters output adjusted accordingly, effecting calibration. This process is repeated for all elements of the array sequentially, starting from the centre of the array. In this paper we consider the reference receiver input signal's accuracy to be limited, in a process which mimics quantisation without adding the attendant noise, denoted q[ ]. We assume that the effects of quantisation noise will be negligible. Although the system is designed explicitly to correct for them, for now we will also ignore the influence of time dependent phenomenon such as component aging and thermal effects and focus on static error correction.

IV. Predicting Calibration Performance

In practical systems hardware can only be produced to finite accuracy and tolerance. Our goal was to derive a closed form

[1]It is important to note that the calibration block shown here (error = σ_c) subsumes both of the individual couplers of the preceding figure.

expression which would give us a statistical prediction of the accuracy of calibration of the array. This prediction is based only upon *a priori* knowledge of the errors of the constituent components of our array system.

A. The Linear Array

In the case of static, single frequency operation, with perfect impedance matching, we define each block of our array radio system to have some predefined average performance, gain A (dB) and phase ϕ°. The actual value of this will vary by some error $\Delta(A,\phi)$ from this ideal. Recalling that the calibration process relies on baseband feedback weighting we also define an error signal $\epsilon(A,\phi)$. Where the input signal to the nth transmitter is a pure sinusoid, $x_n(A,\phi)$, measured by the mth reference with error Δ_{R_m}. It is simple to see from the error signal that perfect array calibration is possible:

$$\epsilon(A,\phi) = (x_1 + \Delta_{R_m}) - (x_n + \Delta_{R_m}) \tag{1}$$

If we now introduce coupler errors $\Delta_c(a,\phi)$ we can see that the accuracy of the calibration of the nth transmitter is degraded by the sum of all of the errors between it and the first transmitter.

$$\epsilon_n(A,\phi) = (x_1 + \Delta_{R_m}) - \left(x_n + \Delta_{R_m} + \sum_{i=1}^{N} \Delta c_i\right) \tag{2}$$

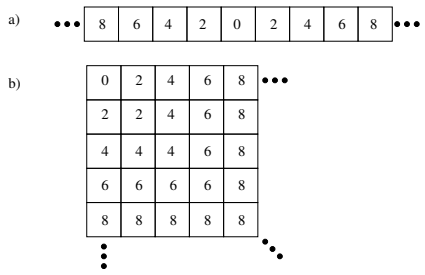

Fig. 5. a) Diagram illustrating graphically the minimum number of calibration paths incurred in calibrating the linear array. b) A similar diagram for a rectilinear array calibrated from the array top-left corner.

Figure 5 a) represents a linear array - each box corresponds to an array element. Using the convention of figure 4 b), the numbers within the boxes represent the sequence and number of coupler calibration path errors accrued during the calibration process. Here calibration starts with the centre-most element. Assuming these coupled paths each have a Gaussian error associated with them and that calibration starts with the centre-most element: An expression for the resultant output error distribution for a N element linear array σ_a, in terms of the coupled calibration path errors σ_c may be derived:

$$\sigma_a^2 = \frac{2}{N-1}2\sigma_c^2 + \frac{2}{N-1}4\sigma_c^2 + ... + \frac{\alpha}{N-1}M\sigma_c^2 \tag{3}$$

Where, in the last term, $\alpha = 1$ if $N-1 = \text{odd}$ elsewhere $\alpha = 2$ and M is N/2 rounded to the nearest integer value. And the reference sensor measurement resolution error contribution is insignificant.

B. The Rectilinear Array

To develop an expression for the rectilinear array we extend this principle to that illustrated in figure 5 b) for an N element square array. Here calibration begins at the top-left hand corner of the array. The numbers therefore denote, not only the sequence that the calibration is performed in, but the number of couplers incurred between the start element (0) and the transceiver being calibrated. As with the linear array, given Gaussian error distribution in coupled path error, by summing and weighting these variances according to the frequency with which they occur, it is possible to calculate the resultant distribution. For the calibration process shown in figure 5 b) the resultant error distribution's phase variance for the array ($\sigma_{\phi_a}^2$) due to this coupled path error is given by:

$$\sigma_{\phi_a}^2 = \sum_{i=2}^{N}\left(\frac{i^2 - [i-1]^2}{N-1}\right)2(i-1)\sigma_{\phi_c}^2 \tag{4}$$

with coupled path phase error variance $\sigma_{\phi_c}^2$ centered around a mean value equal to the phase of the first element. Similarly for the array amplitude error variance:

$$\sigma_{A_a}^2 = \sum_{i=2}^{N}\left(\frac{i^2 - [i-1]^2}{N-1}\right)2(i-1)\sigma_{A_c}^2 \tag{5}$$

with coupler amplitude error variance $\sigma_{A_c}^2$ with the distribution centred around the amplitude of the first element.

V. Simulation

A. Theoretical Comparison

To test the accuracy of these predictions, the calibration scheme representation of figure 5 b) was extended to a rectilinear array as shown in figure 6. In the regime $\Delta_c < \Delta_{Tx}$ and q=14 bits, expressions 4 and 5 were found, to good approximation, to describe array calibration accuracy.

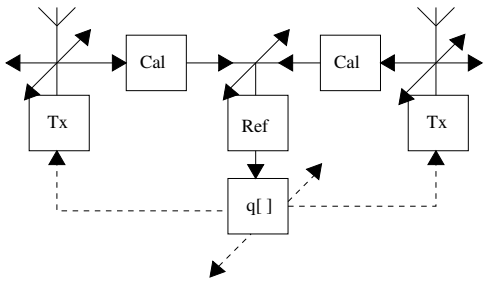

Fig. 6. A block schematic diagram representing the simulation of figure 4 b) modified for the rectilinear case.

This is illustrated in figure 7, which shows how the standard deviation of the array calibration error increases with array size, on this scale the theoretical and simulated results are coincident. Figure 8 shows the mean array error as a function of array size - this again illustrates the accuracy with which our statistical method can predict the array calibration accuracy. The simulation results were obtained by combining the output of 10 000 simulations to obtain statistically significant results.

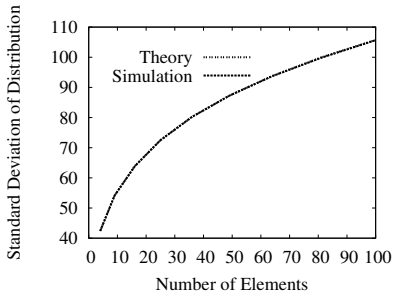

Fig. 7. Comparison of theoretical and simulation predictions for the resultant error distribution given a coupled path with σ_c = 30.

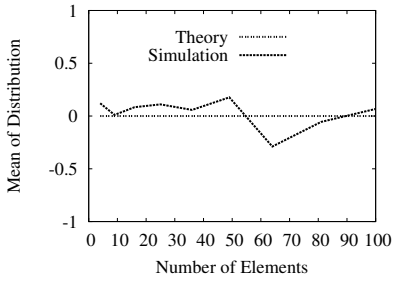

Fig. 8. Comparison of theoretical and simulation predictions for the resultant error distribution given a coupled path with σ_c = 30.

B. Practical Array System Calibration

To generate useful predictions of the performance of a physical array which uses our calibration scheme, values based on available manufacturer's data were attributed to each of the blocks of the simulation scheme of figures 4 b) and 6 . Associated with the phase (ϕ) and amplitude (A) of each S-Parameter (average μ) is a Gaussian error standard deviation, σ, with values as shown in the table below. The initial condition of the input signal to the transmitter block was selected as -20 dBm with a standard deviation of 0.5 dB and uniformly distributed arbitrary phase.

Component	μ_A	σ_A	μ_ϕ	σ_ϕ
Tx S_{21}	50 dB	3 dB	10°	20°
Ref S_{21}	60 dB	3 dB	85°	20°
Cal S_{21}	-40 dB	0.2 dB	95°	2°

These values were selected to reflect low-cost, low quality, commercially available hardware. The specification for the calibration coupler, however, had to be inferred due to the lack of commercially available high balance coupler structures. The coupler phase error is based upon the series connection of a pair of power dividers, each with 3° of peak phase error and an RMS phase error of 1° [2]. Based on the combination of two independent identically distributed random variables this gives a resultant RMS phase error of 1.4°, this was rounded up to 2° to conservatively represent low cost hardware. Similarly an RMS amplitude error of 0.2 dB RMS was calculated for the amplitude imbalance. Work on our own high phase and amplitude balance coupler is on-going and we hope to improve significantly on these figures.

1) Practical Linear Array: To assess the feasibility of our calibration scheme the radiation polar plot feedpoint accuracy of the 30 element linear array of section I, fed by the simulated output of our calibration scheme, was examined. Equation 3 predicts phase and amplitude imbalance of the order of $\sigma = 7.9°$ and 0.69 dB this compares with the values of 8.07 ° and 0.61 dB obtained from 1000 runs of the calibration simulation above. The radiation polar plot of a representative linear array

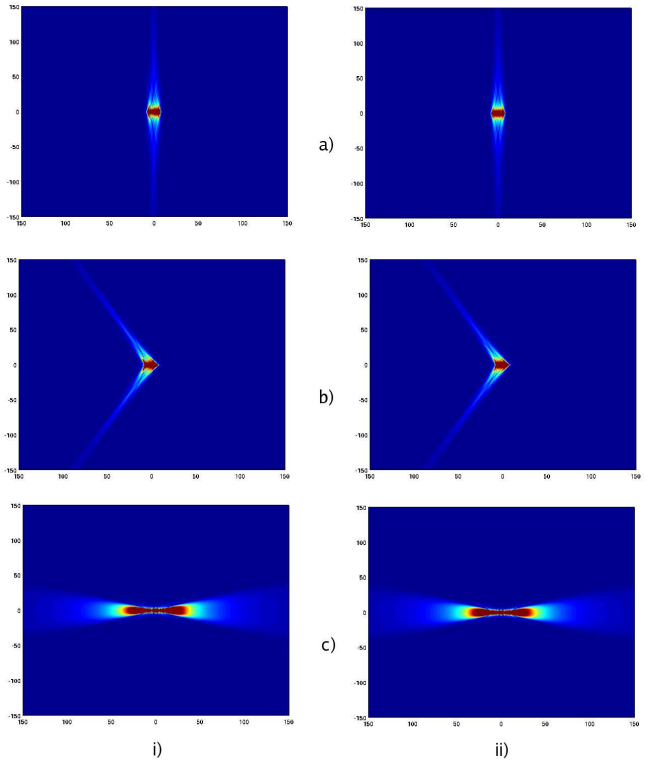

Fig. 9. i) Beamforming performance of the calibration scheme for a 30 element $\frac{\lambda}{2}$ spaced dipole array relative to ii) perfect beamformed output for the same array. a) Broadside, b) 45° and c) endfire radiation patterns shown.

result, in the absence of antenna mutual coupling, is shown in figure 9. Figure 9 i) a) shows broadside, figure 9 i) b) 45° and figure 9 i) c) endfire beamformed radiation. The equivalent ideal beamformed radiation are shown in figures 9 ii) a–c). From these results we can see that the directional beamforming error incurred is unmeasurable and a slight increase in sidelobe level observed in the case of the broadside radiation pattern.

The reason for the lack of beamforming error in figure 9 may be that the larger errors are relegated to the periphery of the array. Anecdotal evidence for this can be seen in Kraus [3], however, the effect of the magnitude of element error distribution on beamforming requires further examination. We will not consider this single array's performance further as our predictions and results are principally concerned with statistical ensembles of arrays. Future work will focus on a method for extracting peak and mean sidelobe levels, as well as directivity error from groups of such plots.

2) Practical Rectilinear Array: To gauge the size of array which can be practically employed using this calibration scheme, the simulated rectilinear array results are plotted as a function of array size in figure 10.

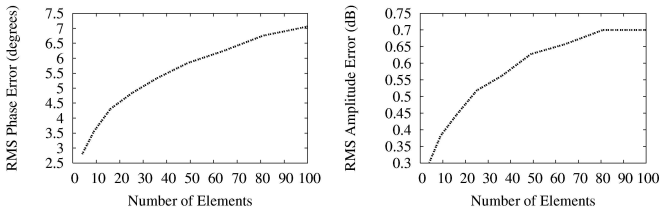

Fig. 10. Phase and amplitude calibration accuracy predicted by the rectilinear array simulation.

To put these figures into context we define two specifications. The first is a stringent phase and amplitude specification based on that of the TSUNAMI (II) array [4], whose amplitude and phasing specifications are maximum 3° peak phase error and 0.5 dB peak amplitude imbalance between any two elements. This is necessary to provide the -30 dB null depth specified for their project. Their hardware embodiment only ever met approximately 10° and 1 dB of imbalance at DCS 1800 frequencies. For a conventional (non-SDMA) tower-top replacement BTS, we define a looser specification of 5° RMS phase error and 1 dB amplitude.

Based on these specifications a provisional coupler accuracy can be generated for a given level of accuracy. Returning to our 30 element rectilinear array requires a coupler balance of 0.42 dB and 2° RMS. This results in a feedpoint calibration accuracy of 1 dB and 5° RMS. Similarly, to satisfy the more stringent SDMA calibration requirement, coupler balance of 0.4° RMS and 0.27 dB is needed, resulting in 0.5 dB and 3° calibration accuracy. Ways of relaxing this coupler balance specification by employing alternative calibration algorithms, are currently under study and will be the subject of future publication.

VI. The Effect of Calibration on Side-Lobe Level

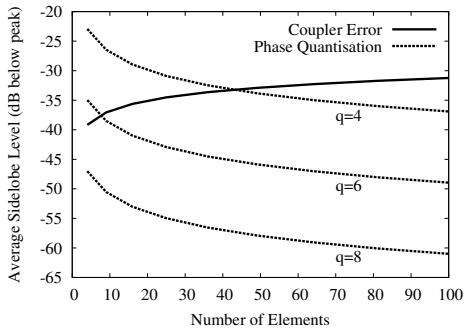

Fig. 11. Sidelobe level contributions due to the calibration scheme (predicted by equations 4 and 5) compared with that due to phase quantisation, note that 14 bit phase quantisation error $\leq$ -80 dB and is not visible on this scale.

To give some indication of the performance and further insight into the behaviour of our calibration scheme in a practical setting, we have taken the predictions of equations 4 and 5 and combined them with the method given by Mailloux [5], to predict the resultant mean sidelobe level due to calibration error. This was undertaken understanding that peak sidelobe level is the key sidelobe parameter for a static cellular systems. Typical cellular BTS antennas require a peak sidelobe level $\leq$ -20 dB, unfortunately we cannot reliably predict the peak sidelobe level from the statistically derived RMS sidelobe level.

Because sidelobe level is a function of array size we can see in figure 11 that the RMS sidelobe level tends towards -30dB below the main lobe radiation for our hypothetical 30 element rectilinear array. This, coincidentally, is the sidelobe level predicted (using the the same method) as for our 30 element linear array. For comparison the RMS sidelobe level due to phase quantisation is also shown in figure 11. This may also serve as some explanation for the limited effect of quantisation rounding, and justification for the exclusion of quantisation noise from our simulation, the average sidelobe level for 14 bit quantisation in the case of the 30 element array is -91.8 dB. The precise influence of quantisation on the accuracy of calibration will be the subject of future study.

VII. Conclusion

In this paper we have introduced a scalable array calibration scheme whose performance is limited by the phase and amplitude imbalance of the passive coupler network employed to couple transmitted power to a reference receiver. Furthermore, we have presented a theoretical basis for the limits of the performance of this system and have confirmed it by simulation in the regime, quantisation greater than 14 bits. This allowed us to derive calibration coupler requirements for both static (2° RMS and 0.42 dB) and SDMA (0.4° RMS and 0.27 dB) beamforming applications. Initial simulation, using the parameters of commercially available components, showed that arrays of up to 100 elements may be produced with a mean sidelobe level over 30 dB below the main lobe of radiation.

Acknowledgment

The authors would like to thank SFI for their generous funding of this project through the CTVR.

References

[1] UBE *Dielectric Ceramic Duplexer, Bandpass Filter Catalog*, Tokyo, Japan, 2006.

[2] Minicircuits, *RF/IC Designers Catalog*, SCN-2-11. New Jersey, USA, 2006.

[3] J.D. Kraus, *Antennas*, 2nd ed. New York, USA: Mc Graw Hill, 1988.

[4] Simmonds, C.M.; Beach, M.A., *"Downlink calibration requirements for the TSUNAMI (II) adaptive antenna testbed,"* Pers., Ind. and Mob. Rad. Comms., 1998. The Ninth IEEE Intl. Symp., vol.3, pp.1260-1264, Sep. 1998

[5] R.J. Mailloux, *Phased Array Antenna Handbook*, 2nd ed. London, England: Artech House, 1999.